Spatiotemporal sensitivity of embryonic heart specification to FGFR signaling in *Drosophila*

V. Yadav[1], N. Tolwinski[2,3] and T. E. Saunders[1,3,4,5,*]

[1] Mechanobiology Institute, National University of Singapore, Singapore
[2] Yale-NUS, National University of Singapore, Singapore
[3] Department of Biological Sciences, National University of Singapore, Singapore
[4] Institute of Molecular and Cell Biology, A*Star, Singapore
[5] Warwick Medical School, University of Warwick, Coventry, United Kingdom
* For correspondence: dbsste@nus.edu.sg

ABSTRACT

Development of the *Drosophila* embryonic mesoderm is controlled through both internal and external inputs to the mesoderm. One such factor is Heartless (Htl), a Fibroblast Growth Factor Receptor (FGFR) expressed in the mesoderm. Htl is involved in shaping the mesoderm at both early and later stages during embryogenesis. How Htl expression levels and timing of signaling affect mesoderm morphogenesis after spreading remains elusive. We have developed an optogenetic tool (Opto-htl) to control the activation of Htl signaling with precise spatiotemporal resolution *in vivo*. We find that the embryo is most sensitive to Htl over-activation within a developmental window of ~4 hours ranging from late stage 10 until early stage 13, which corresponds to early stages of heart morphogenesis. Opto-htl restores heart cells in *htl* mutants upon light activation, independent of its role in early mesoderm shaping events. We also successfully generated spatially distinct regions of Htl activity in the mesoderm using light-sheet microscopy. The developing tissue was unable to correct for the ensuing asymmetries in cell fate. Overall, Opto-htl is a powerful tool for studying spatiotemporal regulation of Htl signaling during embryogenesis.

INTRODUCTION

Morphogenetic events are tightly controlled in space and time (Wartlick *et al*., 2011; Ebisuya & Briscoe, 2018; Huang & Saunders, 2020). Throughout development, cells propagate,

34 migrate, and differentiate to form specialised structures in a highly regulated manner. Such
35 self-organisation within the embryo is dictated by numerous signaling events, some of which
36 are highly conserved across organisms (Wangler *et al*., 2015; Beira & Paro, 2016; Li &
37 Elowitz, 2019). Many of these signaling pathways interact with each other, generating complex
38 network interactions and are interpreted differently by cells based on their competence to
39 respond (Perrimon *et al*., 2012; Sagner & Briscoe, 2017; Yin *et al*., 2018; Li & Elowitz, 2019).
40 These signaling networks are regulated in both space and time throughout morphogenesis to
41 ensure that development is robust and reproducible (Amourda *et al*., 2017; Huang *et al*., 2017;
42 Zinner *et al*., 2020).
43
44 A crucial signaling pathway in regulating cell behaviour during development is the highly
45 conserved Fibroblast Growth Factor Receptor (FGFR) pathway (Sopko & Perrimon, 2013).
46 FGFRs are transmembrane proteins that belong to the receptor tyrosine kinase family. Ligand-
47 binding leads to FGFR homo-dimerisation, initiating trans-phosphorylation events which
48 ultimately activates transcription of several target genes (Fantl *et al*.,1993). This transcriptional
49 response regulates different cellular responses, such as changes in cell morphology,
50 proliferation, adhesion, migration and differentiation (Spivak-Kroizman *et al*., 1994;
51 Mohammadi *et al*., 1996; Thisse & Thisse, 2005; Teven *et al*., 2014; Mele & Johnson, 2020).
52 Due to their involvement in key cellular processes, FGFRs when mutated can promote cancer
53 development and progression (Turner & Grose, 2010; Wesche *et al*., 2011; Presta *et al*., 2017).
54
55 There are two known FGFRs in *Drosophila* that control distinct developmental processes,
56 *heartless* (*htl*) and *breathless (btl)*. These bind three ligands in total - Pyramus, Thisbe and
57 Branchless (Stathopoulos *et al*., 2004; Kadam *et al*., 2009). This compares with four known
58 FGFRs and at least 22 associated ligands in humans that bind each other in several different
59 combinations (Ornitz & Itoh, 2015). The small number of receptor-ligand combinations makes
60 *Drosophila* an excellent system to explore the basic interactions underlying FGFR action. In
61 *Drosophila, htl* expression is important for proper development of several mesoderm derived
62 tissues, including the heart and muscles (Beiman *et al*., 1996; Gisselbrecht *et al*., 1996;
63 Shishido *et al*., 1997). *btl* expression is required for proper morphogenesis of the trachea
64 (Klambt *et al*., 1992; Reichman-Fried *et al*., 1995). Both Htl and Btl are essential in driving
65 proper migration of mesodermal, glial, and tracheal cells (Muha & Müller., 2013). For instance,
66 Htl plays a role in the spreading of the mesoderm over the ectoderm to form a monolayer during

early stages of embryogenesis (Wilson *et al*., 2004; Wilson *et al.*, 2005; McMahon *et al*., 2010; Bae *et al*., 2012). Uniform spreading of the mesoderm is crucial for proper cell-fate specification of different cell types within the mesoderm at later stages (Stathopoulos *et al*., 2004; Kadam *et al*., 2009). In *htl* mutants, mesoderm cells fail to undergo proper spreading and form irregular and multilayer arrangements. This lack of structure prevents mesodermal cells from receiving precise spatial cues from the ectoderm. Later in development, Htl is also involved in the specification of different cell types derived from the mesoderm (Michelson *et al*., 1998). *htl* null mutants lack precursors of pericardial and heart cells, have defects in visceral mesoderm, and show reduced, irregular muscle patterns (Beiman *et al*., 1996; Stathopoulos *et al*., 2004; Kadam *et al*., 2009).

The role of FGFR in cell fate specification has been extensively studied (Carmena *et al*., 1998; Ciruna & Rossant., 2001; Mandal *et al*., 2004). While previous work has provided detailed insights into how Htl controls the movement of mesodermal cells during the spreading phase (McMahon *et al*., 2008), the *in vivo* dynamics of Htl action within the developing mesoderm remain elusive after the initial stages of spreading. Genetic perturbations of *htl* offer only a limited exploration of the spatiotemporal range of Htl activity. In recent years, the use of optogenetics to tune signaling pathway responses has become a powerful tool *in vivo* (Huang *et al*., 2017; Kaur *et al*., 2017; Viswanathan *et al.*, 2019; Johnson *et al*.,2020). Optogenetic approaches enable precise spatiotemporal tuning of target activity, enabling *in vivo* signaling dynamics to be dissected.

Here, we utilised an optogenetic tool (termed Opto-htl) to activate Htl signaling in a spatiotemporally controlled manner during *Drosophila* embryo development. Upon illumination with 488nm light, Opto-htl functions as a constitutively active receptor, capable of activating downstream factors of the FGFR pathway, such as the extracellular signal regulated kinase (Erk). Opto-htl restored a significant number of heart cells within a *htl* mutant upon light activation, though it did not fully rescue the mutant phenotype. Constitutive activation in the mesoderm of the wild-type led to several developmental defects, the severity of which varied with changes in light intensity, timing, and spatial organisation of the light exposure. We identified a time window of sensitivity to FGFR over-activation (stage 10 till late stage 12 of embryogenesis), illumination during which was both necessary and sufficient

99 to induce the phenotypic defects. Together, these results demonstrate sensitivity of the Htl-
100 dependent processes (particularly heart formation) to over-activation of Htl.
101
102 **RESULTS**
103
104 **Opto-htl can stimulate FGFR activity**
105
106 To generate an *in vivo* optogenetic tool for FGFR activation, we utilised Cryptochrome2
107 (CRY2), a light-interacting molecule that undergoes dimerisation upon exposure to 488nm blue
108 light (Yu *et al*., 2009). The cytoplasmic domain of *htl* was fused with CRY2-mCherry and the
109 resulting fusion protein (termed Opto-htl) was anchored to the membrane by a myristoylation
110 (myr) signal sequence (Kim *et al*., 2014). Light exposure induces dimerisation of CRY2,
111 bringing two receptor molecules together and triggering a phosphorylation cascade, which
112 should lead to ligand-independent activation of target genes downstream of the receptor (Fig.
113 1A).
114
115 We used Twi-Gal4 to drive Opto-htl (Twi-Gal4>UAS-htl-CRY2-mCherry) (Fig. 1B, top) in
116 the mesoderm. We validated that our construct was expressed in the mesoderm and mesoderm-
117 derived tissues at different stages throughout embryogenesis (Fig. 1B). Live imaging showed
118 that expression levels remained low until stage 10 but subsequently increased and were
119 maintained in the mesoderm throughout embryogenesis (Movie S1). Twi-Gal4>Opto-htl
120 embryos maintained in the dark throughout embryogenesis hatched with similar frequency to
121 wild-type (OreR) embryos (Movie S3). However, upon constant light exposure (Methods) from
122 stage 5 onwards, there was a significant drop in hatchability and 97% of embryos died before
123 hatching (Fig. 1C). These embryos developed up until the later stages of embryogenesis before
124 dying unhatched (Movie S3).
125
126 Next, we tested the constitutive activation of the FGFR pathway via Opto-htl. We used the
127 phosphorylation of Erk as a readout for the MAPK/Erk pathway downstream of FGFR (Gabay
128 *et al*., 1997). Erk activation to doubly phosphorylated Erk (dpErk) leads to transcription of
129 several target genes that regulate growth and proliferation (Lavoie *et al*., 2020). We tested for
130 differences in the levels of dpErk in Opto-htl embryos kept under dark and light conditions.
131 We illuminated Twi-Gal4>Opto-htl embryos up until the end of germ band elongation (late

132 stage 10 / early stage 11), then fixed and stained them with anti-dpErk antibody alongside
133 embryos kept in the dark. We observed an increase in dpErk levels in embryos exposed to light
134 as compared to the ones fixed and stained at a similar stage in the dark (Fig. 1D). We also
135 tested Erk activation in the hindgut epithelium (ectoderm-derived) which does not express high
136 levels of dpErk in wild-type conditions. We used Byn-Gal4 to express Opto-htl in the hindgut
137 epithelium and again tested for dpErk levels under dark and light conditions (Fig. 1E).
138 Comparing the dpErk intensity for dark and light conditions in both tissues, dpErk levels were
139 significantly increased upon light activation (Fig. 1F-G). We conclude that Opto-htl can be
140 used to induce Erk activation *in vivo* upon illumination.
141
142 **Opto-htl can induce heart cells in a *heartless* mutant**
143
144 To further test the functionality of Opto-htl, we expressed it against a null *htl* mutant
145 background to explore the extent of rescue of phenotypes at different stages upon light
146 illumination. Homozygous mutants for *htl* undergo improper spreading of mesoderm cells at
147 stage 10 forming irregular and multilayer arrangements (Stathopoulos *et al*., 2004), lack
148 pericardial precursors, a proper muscle structure, pattern and, as the name suggests, fail to form
149 a proper heart (Beiman *et al*., 1996) (Fig. 2A). A previous tool to induce *htl* over-expression,
150 htl-λ (Michelson *et al*., 1998; Wilson *et al*., 2005), was able to partially rescue the *htl* mutant,
151 with some Eve-positive cells (precursors for pericardial and dorsal muscles) in the mesoderm
152 restored.
153
154 We tested for rescue of heart cells at stage 16 in homozygous *htl* mutants expressing Twi-
155 Gal4>Opto-htl with and without light activation. Tinman (Tin) is a transcription factor required
156 for the specification of all heart cells and a subset of muscles (Bodmer, 1993). At stage 15/16,
157 Tin is expressed in a major portion of the cardioblasts and pericardial cells (Alvarez et al.,
158 2003). We found that homozygous embryos maintained in light showed restoration of Tin-
159 positive heart cells at stage 16 when compared to embryos kept in the dark (Fig. 2B-C). In
160 comparison, in wild-type embryos, there are around 104-Tin-positive cells in hemisegments
161 A2-A8 (52 cardioblasts and pericardial cells each) at late stage 15/16 (Alvarez et al., 2003).
162 Although Tin-positive cells were greatly increased under light activation of Opto-htl in *htl* null
163 embryos, there was substantial variation in their spatial arrangement between embryos. The
164 Tin-positive cells were located near the embryonic midline, but they failed to form a coherent

heart structure. This is likely a consequence of embryos failing to undergo uniform mesoderm spreading over the ectoderm early on.

Opto-htl showed no rescue of phenotypes during early stages of development (Fig. S1). Since Opto-htl expression levels are generally low during early stages (Movie S1), it is possible that rescue during this stage requires higher levels of FGFR signaling than we currently achieve. These results are consistent with previous findings that Htl-dependent cell fate decisions in the mesoderm after stage 10 are decoupled from its role in mesoderm spreading (Michelson *et al.*, 1998), though formation of robust organs requires synergy between both processes.

Activation of Opto-htl induces ectopic Tin-positive cardioblasts

Light activation of Opto-htl in the wild type mesoderm interfered with embryonic development, leading to a significant increase in lethality. We focused on the effect of Opto-htl activation on the development of mesoderm-derived tissues, particularly the heart. The heart in wild-type and Opto-htl embryos kept under dark is composed of two rows of cells (Fig. 3A left) with a repeated pattern of four Tin-positive and two-Seven-up (Svp) positive cells (Ahmad, 2017; Vogler & Bodmer, 2015) (Fig. 3B, top). The cells comprising these two rows are specified on both lateral sides of the embryo by the end of stage 12 after which they start migrating towards each other and match in a highly precise fashion (Reim & Frasch., 2010, Zhang *et al.*, 2018; Zhang *et al.*, 2020) (Fig. 3B top, Movie S4). Upon illumination, the stage 16 heart in Twi-Gal4>Opto-htl embryos showed a significant increase in the number of cardioblasts (Fig. 3A right and Fig. 3B bottom). There was an increase in the number of cardioblasts per hemisegment, but with substantial variation between embryos (Table 1). The clusters still had Svp-positive cells appearing in doublets, identifiable by reduced Fasciclin-III (Fas3) expression and morphology (Zhang *et al.*, 2018) (asterisk in Fig. 3B) as in wild-type embryos, but they no longer matched with their contralateral partners. In some cases, the heart structure even becomes discontinuous (Movie S5). The observed asymmetries in the light-activated Opto-htl embryos suggested that the ectopic heart cells were generated asymmetrically between the contralateral sides of the embryos. Some embryos even developed multiple branches emanating from what appeared to be the primary heart vessel (arrowhead Fig. 3B).

198 **Activation of Opto-htl disrupts mesoderm-derived muscle formation**

199

200 In wild-type embryos, the dorsal muscles - DA1 muscles - are initially flower like structures
201 formed from a cluster of Eve-positive cells around both sides of the heart (Han & Bodmer.,
202 2003; Schwarz *et al*., 2018). Upon staining with Eve antibody, we observed that the DA1
203 muscle precursors are completely missing from Opto-htl embryos kept under light (Fig. 3C,
204 Eve). These embryos also showed a reduced number of muscle-forming Mef2 positive cells
205 (Fig. 3C, brackets) (Mef-2 is a key transcription factor that marks and directs proper
206 specification of the heart and muscle cell types (Bour *et al*., 1995; Lilly *et al*., 1995)). We next
207 visualised the muscle patterns at stage 16 using the mCherry signal marking Opto-htl. In wild-
208 type embryos and in Opto-htl embryos kept in dark, the somatic muscles were arranged and
209 attached to the body wall in regular patterns (Zhou *et al*., 2019) (Fig. 3D). This pattern was
210 disrupted in Opto-htl embryos kept under light, with the muscles appearing diffused and
211 disrupted (Fig. 3D). Overall, we see that over-activation of Opto-htl leads to a loss of structural
212 organisation within mesoderm-derived tissues.

213

214 **Opto-htl allows spatially precise activation of Htl signaling within the developing**
215 **mesoderm**

216

217 We used a light-sheet microscope to generate a spatially restricted region of Opto-htl activation
218 within a developing embryo. Since the light-sheet illuminates and collects the signal from a
219 single optical section at a time, we are able to partition a given embryo into illuminated and
220 non-illuminated sections. (Kaur *et al*., 2017). A Twi-Gal4>hand::GFP; Opto-htl embryo was
221 mounted such that the illumination plane was parallel to the long-axis of the embryo. To
222 generate spatially heterogeneous activation of Opto-htl, we scanned the Opto-htl embryos with
223 the 488nm laser to a depth of ~35um from the embryo surface on one lateral side, so as to
224 illuminate the heart precursors on only one side of the embryo (Fig. 4A). At stage 16, we
225 imaged the embryo from the dorsal side to image the heart and compared Hand::GFP signals
226 from the illuminated and non-illuminated sides. We observe a striking difference between the
227 number of heart cells on both sides, with the non-illuminated side resembling the dark
228 condition phenotype while the illuminated side showed multiple ectopic cardioblasts (Fig. 4B,
229 asterisk).

230

231 We observed ectopic cardioblasts in the illuminated side immediately after the end of
232 illumination at stage 13 (Fig. 4C, left). By the end of stage 15 (Fig. 4C, right), the non-
233 illuminated side resembled the wild type embryo in its arrangement and number of heart cells
234 while the illuminated side had substantial ectopic cardioblasts arranged irregularly along the
235 embryonic midline. These results suggest that the two lateral sides of the mesoderm develop
236 independently from each other, and they cannot correct for defects in the formation of their
237 contralateral partner which is consistent with the fact that the mesodermal cells do not mix
238 extensively along the lateromedial axis and their spatial information with respect to one another
239 is more or less conserved (Ortega & Hartenstein, 1985).
240
241 **Severity of Opto-htl induced phenotypes is dosage dependent**
242
243 We observed the aforementioned phenotypic defects in Opto-htl embryos upon continuous and
244 uniform illumination at a fixed intensity of 1mW (measured at the sample plane). Next, we
245 varied the dosage of signaling via Opto-htl by illuminating Opto-htl embryos with different
246 light intensities using a Nikon LED light base as the light source. We used light intensities at
247 2 mW, 1 mW, 0.25 mW, 0.1 mW, and 0.01 mW (measured using an intensity power meter set
248 at the 488nm range) for illuminating Twi-Gal4>hand::GFP; Opto-htl embryos from stage 5 up
249 until stage 15/16 and then imaged the heart in each embryo. Hand::GFP is expressed at stage
250 16 in all the heart cells and the adjacent visceral mesoderm. In Fig. 5A we depict the most and
251 least defective heart images at each intensity, based on the number of ectopic cardioblasts. At
252 low intensities (0.01mW), the least defective embryos closely resembled embryos maintained
253 in the dark condition (Fig. 5B), with only a few ectopic cardioblasts. At 0.1mW, ectopic
254 cardioblasts were more apparent in some embryos, though the overall structure still resembled
255 the non-illuminated embryos. For intensities 0.25mW and above, the heart defects were
256 marked, with major structural changes to the heart vessel (branching, inconsistent matching).
257
258 After imaging the embryos at stage 16, we let them develop further and scored their
259 hatchability. We found that increased intensity led to lower survival rates. At 0.1mW exposure,
260 we observe a survival rate of around 57% as compared to a 100% lethality observed at intensity
261 values of 1mW or higher (Fig. 5C). Despite significant ectopic cardioblasts, 52% of the
262 embryos illuminated at 0.25mW still managed to hatch, possibly due to reduced severity of
263 some other defects at lower intensities.

264

265 We compared these results with the other constitutively active form, htl-λ (Michelson *et al*.,
266 1998; Wilson *et al*., 2005). htl-λ did not induce lethal phenotypic defects when expressed in
267 the mesoderm. Tin and Eve patterns at stage 15 in Twi-Gal4>htl-λ embryos showed only small
268 phenotypic variation from wild-type patterns (Fig. S3). The heart phenotype observed for htl-
269 λ resembled that of Opto-htl embryos at lower intensity illuminations (<0.1mW). Of course,
270 differences between the scales of action for the two constructs cannot be ruled out. At higher
271 light activation, we see stronger phenotypes in the Opto-htl embryos as compared to htl-λ. Our
272 results suggest that specification of the cardiac vessel within the mesoderm is highly sensitive
273 to FGFR activity levels.

274

275 **Embryo development is sensitive to Opto-htl activation only during stages 10-12**

276

277 In the early embryo, Htl plays an important role in regulating mesoderm spreading (Wilson *et*
278 *al*., 2005; McMahon *et al*., 2010), but the dynamics of its activity later in development are less
279 well known. We used Opto-htl to activate Htl signaling during distinct developmental time
280 windows to disentangle its early and later effects on embryo development and to test when the
281 developing mesoderm is most sensitive to Htl over-activation.

282

283 We illuminated Twi-Gal4>Opto-htl embryos during three separate time windows (Fig. 6A): (i)
284 from stage 5 to stage 10 (~2.5 hours), during which the presumptive mesoderm forms the
285 ventral furrow and undergoes spreading over the ectoderm to form a monolayer; (ii) from late
286 stage 10 to late stage 12 (~4 hours), during which the specification of the presumptive
287 mesoderm into different cell types occur; and (iii) from stage 13 up to stage 16 (~4 hours),
288 during which cardioblasts migrate to the embryo midline and form the heart. We observe that
289 nearly all embryos illuminated during windows (i) and (iii) hatch. However, almost all embryos
290 illuminated between stages 10 and 12 fail to hatch (Fig. 6A). As previously stated, Opto-htl
291 levels at early stages i.e. during time window (i), can only be detected by anti-mCherry
292 antibody staining, suggesting low expression levels (Movie S1).

293

294 We next performed illuminations during more fine-tuned developmental windows (Fig. 6B-C,
295 Table 2A-B). We see a sharp transition in survivability around stage 12 where embryos
296 illuminated prior to stage 12 show high lethality, and embryos illuminated only after stage 12

297 show high survivability (Fig. 6B). Performing the opposite light illumination protocol,
298 embryos illuminated until stage 10 but then kept in the dark all hatched. Embryos illuminated
299 until stage 11 had a survivability of around 50%. Developmental processes around stage 11-12
300 appear to be especially sensitive to Opto-htl activation. The specification of different cardiac
301 progenitors occurs during this stage (Reim & Frasch., 2010). To determine what defects were
302 induced by illumination of Opto-htl during time window (ii), we let embryos illuminated during
303 this window continue to develop in the dark from stage 13 onwards and fixed them at stage 16.
304 We observed that these embryos had ectopic Mef-2 positive cardioblasts (Fig. 6D, arrows),
305 similar to Opto-htl embryos illuminated throughout development. Further, the Mef-2 positive
306 muscle cells were also reduced as seen in the body wall muscles (Fig. 6D , brackets).
307
308 We observed that activation of Opto-htl during the developmental period from late stage 10
309 until late stage 12 was both necessary and sufficient to induce the described mesodermal
310 defects. This window is crucial for heart morphogenesis and requires precise levels of FGFR
311 activation to ensure proper cell fate specification and robust development (Reim & Frasch,
312 2010). In contrast, later developmental processes (post stage 13) appear to be able to tolerate a
313 much higher range of Htl activity, possibly because cell-fate specification has already
314 happened by this time and/or cells can buffer any increased Htl activity.
315
316 **DISCUSSION**
317
318 The embryonic mesoderm gives rise to a diverse range of cell types that form the heart, visceral
319 musculature, haemocytes and the fat body. Htl plays a crucial role in shaping the mesoderm by
320 ensuring (i) uniform spreading of the mesoderm over the ectoderm and (ii) subsequent fate
321 specification of different tissue precursors (Michelson *et al*., 1998; Wilson *et al*.,2000;
322 Stathopoulos *et al*., 2004; Kadam *et al*., 2009). Here, we have demonstrated the use of an
323 optogenetic tool (Opto-htl) to study spatiotemporal regulation of Htl signaling by controlling
324 its level of activation *in vivo* along with precisely defined spatial and temporal windows. We
325 found that the embryo is highly sensitive to Htl over-activation during the time window from
326 late stage 10 till end of stage 12 (early stages of heart morphogenesis). Illumination from stage
327 13 onwards did not result in any remarkable defects (Fig. 6). Within the stage 10 to 12 window,
328 the severity of the phenotype decreased with decreasing light intensity (Fig. 5A). Opto-htl
329 provides a distinct advantage over previous studies of Htl over-activation, as it allows careful

330 tuning of the strength of the pathway response. We can induce a stronger signaling dosage
331 response in the mesoderm from stage 10 by increasing the light intensity of illumination.
332
333 There was no apparent increase in the total number of mesodermal cells upon light activation
334 in Twi-Gal4>Opto-htl embryos observed at stage 11(Fig. S2). By stage 13, however, we see
335 an increase in the number of Hand::GFP-positive cells in these embryos when exposed to light
336 (Movie S5B-C and Fig. 4C, compare the non-illuminated and illuminated sides). We currently
337 do not have a live reporter for cardioblasts with clear expression at stage 10-12 (Hand::GFP
338 comes up in stage 13). In related work, we are developing new lines to explore the dynamics
339 of early heart formation. We can then unravel whether the changes in cell number are related
340 to over-proliferation of Tin-positive cardioblasts or switches in cell identity of other
341 mesodermal cells and also decipher the exact timing of these events during development.
342
343 Surprisingly, illuminated Twi-Gal4>Opto-htl embryos at 1mW intensity do not show an
344 increase in number of Eve-positive precursors (at stage 11) that form future pericardial cells
345 and DA1 muscles. This contrasts with the htl−λ construct, that induced additional Eve-positive
346 precursors at stage 11 but did not result in a lethal phenotype at later stages (Fig. S3). In Twi-
347 Gal4>Opto-htl embryos, Eve-positive DA1 muscles at stage 16 are completely missing from
348 light-activated (1mW) embryos at stage 16 (Fig. 3C). At low light activation, our Opto-htl
349 phenotype was similar to that of htl-λ with respect to the number of ectopic Tin-positive heart
350 cells observed at stage 16 (Fig. S3, asterisk). It is possible that at higher light intensity of 1mW,
351 Opto-htl over-activation of the FGFR pathway is inducing conversion from a muscle cell fate
352 to a cardiac or pericardial cell fate; *i.e*. Mef-2 positive muscle founders adopting a Tin-positive
353 cardioblast fate and Eve-positive dorsal muscle cells adopting a pericardial fate. Therefore,
354 Opto-htl potentially enables fine-tuning of FGFR-dependent cell fate decisions within the
355 developing mesoderm. This opens up the possibility to explore the role of *htl* activity in
356 controlling mesoderm cell behaviour with greater precision and across a greater range than
357 possible with other tools.
358
359 There are several different pathways downstream of Htl (Ras/Raf/MAPK, PLCγ, PI3/AKT)
360 characterised based on their molecular components and the response they generate (Ornitz &
361 Itoh., 2015). Each pathway activates transcription of a set of different genes generating cellular
362 responses such as proliferation, differentiation, migration, cell survival, and apoptosis. The

363 MAPK pathway activation plays an important role in development of several different cancer
364 types (Roskoski., 2019). We compared the developmental effect of constitutive activation at
365 the receptor level with Opto-htl (potentially activating all downstream pathways) to activation
366 of only the Ras/Raf/MAPK pathway in the mesoderm by driving Opto-SOS (Johnson *et al*.,
367 2017) with Twi-Gal4. Upon illumination, we observe similar phenotypes in the heart as with
368 Opto-htl; abundance of Tin-positive cardioblasts and loss of DA1 muscles (Fig. S4). The
369 phenotypes are pronounced at 4.5mW illumination intensity, at which no DA1 muscles are
370 observed and there is an abundance of Eve-positive pericardial cells and Tin-positive
371 cardioblasts. At lower intensities, some of the DA1 structure is maintained. Hyperactivation of
372 the Ras/Raf/MAPK pathway alone leads to phenotypes similar to Opto-htl in the mesoderm.
373 This suggests that MAPK signalling dosage is critical in regulating cell proliferation and cell
374 fate specification events in the mesoderm during stages 10-12.
375
376 We observed that Opto-htl can restore Tin-positive cardioblasts in *htl* null mutants upon light
377 activation (Fig. 2C). Specification of Tin-positive heart precursors relies on the dorsal-most
378 mesodermal cells receiving cues from Decapentaplegic and Wingless (Reim & Frasch., 2010),
379 which emanate from the neighbouring ectodermal tissue. In *htl*-null mutants, mesoderm
380 spreading is defective, but some cells still lie near to the neighbouring ectoderm. This likely
381 explains how Opto-Htl is able to activate *tin* expression in *htl* null mutants and why the
382 resulting pattern of Tin-positive cardioblasts is heterogeneous. This is consistent with the role
383 of Htl in heart cell specification, independent from its role in mesoderm spreading (Michelson
384 *et al*, 1998).
385
386 Our results suggest that Htl-dependent cell fate decisions are highly stage specific and dosage
387 dependent. An increase in dosage leads to variations in different cell types of the heart and
388 muscle lineage. These events are specifically restricted to a time window for Htl over-
389 activation between late stage 10 and early stage 13, though recall that the lower time bound is
390 uncertain due to relatively lower expression levels of Twi-Gal4>Opto-htl at early stages. Using
391 Opto-htl to control several parameters of FGFR activation - dosage, spatial region of activation,
392 and timing of activation - we have provided insight into different modes of Htl action in the
393 developing mesoderm. In future work, we aim to fine tune these parameters further, to study
394 how they affect cell fate changes *in htl* null embryos.
395

FGFR signalling plays a crucial role in the development and maintenance of several different organ systems in humans (heart, lungs, brain, skeletal muscles, etc.) and is also a target in disease therapies (Xie *et al.,* 2020). There is evidence from animal studies that FGFR signal activation has potential for use in tissue regeneration and repair (Engel *et al*., 2006; Korf-Klingebiel *et al*., 2011; House *et al*., 2015). Optogenetic control over signalling pathways allows us to fine tune their activation or deletion in a highly controlled spatiotemporal manner. Studying the conditional effects of these manipulations on development and disease pathogenesis has the potential to lead to novel therapeutics.

Acknowledgements:

We thank Kenji Matsuno, Maria Leptin and Zhe Han for fly lines. We thank Manfred Frasch, James Sharpe and Eileen Furlong for the Tinman, Eve and Mef-2 antibodies respectively. We acknowledge members of the Saunders laboratory for fruitful discussions. This work was supported by a Singapore Ministry of Education AcRF Tier 3 Grant (MOE2016-T3-1-002).

Author Contributions:

All authors designed and planned the study. VY performed all experiments and data analysis, with guidance from NT and TES. VY and TES wrote the initial manuscript, will all authors contributing to the final manuscript.

418 **Materials and Methods:**

419

420 **Fly stocks, husbandry and genetics**

421 UAS-htl-Cry2mCherry construct was generated using Gibson assembly (NEB) of four
422 fragments: pPW vector backbone digested and purified, synthesized src42A myristoylation
423 (myr) signal sequence, PCR amplified cytoplasmic region of htl/btl from cDNA, PCR
424 amplified CRY2mCherry sequence from the AddGene plasmid #26866 (Kennedy *et al*., 2010).
425 The recombinant plasmid was sent to BestGene Inc for P-element transformation. Twi-Gal4
426 (BDSC58804, BDSC2517) was used to drive expression in the mesoderm and Byn-
427 Gal4>UAS-myr-GFP was used to drive expression in the hindgut (kindly provided by Kenji
428 Matsuno). To mark the heart cells for live imaging, we used Hand::GFP (GFP driven by the
429 Hand cardiac and hematopoietic (HCH) enhancer (Han, 2006)) and formed a stable line:
430 Hand::GFP;UAS-htl-Cry2mCherry.

431

432 For the rescue experiments, UAS-htl-Cry2mCherry on 2nd chromosome was combined with the
433 htl^{AB42} null mutant on 3rd chromosome (BDSC 5370). Similarly, Twi-Gal4 on 2nd chromosome
434 (BDSC2517) was combined with htl^{AB42} null mutant to form a stable line. UAS-htl-
435 Cry2mCherry; htl^{AB42} / TM3-ftz-lacz virgin females were crossed to Twi-Gal4; htl^{AB42} / TM3-
436 ftz males resulting in 25% homozygous mutant embryos expressing Twi-Gal4>UAS-htl-
437 Cry2mCherry. All fly lines were raised at 25°C.

438

439 **Identification of homozygous *htl* mutant embryos for rescue experiments**

440 For the rescue crosses, a balancer chromosome carrying a lacZ-transgene was used. lacZ
441 expression was driven by the ftz-promoter and was detected in embryos using anti- β-Gal
442 antibody (DSHB 40-1a). For cross-section staining, lacZ-positive and lacZ-negative embryos
443 were sorted under a dissecting microscope based on the β-gal staining pattern prior to cutting
444 in 70% glycerol using a 25-gauge needle.

445

446 **Immunostaining**

447 Embryos were collected at the desired stages, then dechorionated using bleach and fixed in
448 heptane saturated with 37% paraformaldehyde (PFA) for 50 minutes. The vitelline membrane
449 was subsequently removed using a needle. Prior to immunostaining, the embryos were blocked
450 in 10% BSA-PBS. Antibodies used were mouse anti- β-Gal (1:100, DSHB), rabbit anti-

451 mCherry (1:100, Abcam), guinea pig anti-Eve (1:800, kindly provided by James Sharpe), rabbit
452 anti-dpERK (1:100, CST), mouse anti-fas3 (1:300, DSHB), Rabbit anti-tin (1:1000, kindly
453 provided by Manfred Frasch), mouse anti-myosin heavy chain (1:100, DSHB), rabbit anti-
454 mef2 (1:800, kindly provided by Eileen Furlong). Primary antibodies were detected with Alexa
455 Fluor-labelled secondary antibodies (1:500; LifeTech). Embryos were mounted in AquaMount
456 (PolySciences, Inc.) and imaged using a Zeiss LSM710 microscope with a C-Apochromat 40x
457 water-immersion objective or a Nikon A1-RS scanning confocal microscope with 40x water-
458 immersion objective. For dpERK intensity comparisons, both dark and light condition embryos
459 were collected, stained and imaged under same conditions (antibody dilutions, laser power,
460 etc).
461
462 **Illumination experiments**
463 To score hatchability, embryos were imaged on a bright-field stereomicroscope at 25°C. To
464 maintain the dark condition where needed, embryos were observed with the light source
465 covered with amber paper to block 488nm light. For illuminating embryos, we used a Nikon
466 LED light base as the light source and measured different light intensities using an intensity
467 power meter set at the 488nm range. All experiments were carried out at 1 mW (measured at
468 the sample plane) unless otherwise stated. For different time-window illuminations, stage 5
469 embryos were collected in the dark condition (488nm light blocked by amber paper) and then
470 exposed to light. For keeping embryos in dark for recovery after illumination, we used a box
471 covered with aluminium foil. For staining experiments, dark and light condition embryos were
472 fixed and stained simultaneously at exactly similar stages. All embryos were collected and
473 staged according to Ortega & Hartenstein (1985).
474
475 **Light-sheet microscopy for spatially controlled activation**
476 Embryos were dechorionated using bleach, mounted into a capillary containing 1% low-
477 melting agarose (Sigma) in an upright position and imaged on a Z.1 light-sheet fluorescence
478 microscope (Carl Zeiss, Germany) using a 40x water immersion objective. The light-sheet
479 microscope was equipped with 30 mW 488 nm and 20 mW 561 nm lasers with BP505–545
480 and LP585 emission filters respectively. Embryos were imaged using dual-side illumination
481 by a light-sheet modulated into a pivot scan mode. The 488 nm excitation laser was used at 6%
482 power with 7.5ms exposure time and the 561 nm excitation laser was used at 13% laser power
483 with 20ms exposure time. For control embryos, only the 561 nm laser was used for scanning.

For spatial control of activation, embryos were mounted vertically and scanned with the 488nm laser from the lateral side such that the light-sheet was parallel to the plane of the embryo. ~35um of slices from the embryo surface were scanned so as to illuminate the heart precursors on only one side of the embryo. We scanned embryos with the 488nm laser from stage 10 till stage 13 and then we let embryos develop in the dark until stage 16 (no scanning with 488nm laser). At stage 16, we scanned the dorsal side of the embryos to image the heart and compared signals from the illuminated and non-illuminated sides.

References

Ahmad, S. M. (2017). Conserved signaling mechanisms in Drosophila heart development. *Developmental Dynamics*, *246*, 641–656.

Alvarez, A. D., Shi, W., Wilson, B. A., & Skeath, J. B. (2003). pannier and pointedP2 act sequentially to regulate Drosophila heart development. Development, 130, 3015-3026.

Amourda, C., & Saunders, T. E. (2017). Gene expression boundary scaling and organ size regulation in the Drosophila embryo. *Development, growth & differentiation*, 59, 21-32.

Bae, Y. K., Trisnadi, N., Kadam, S., & Stathopoulos, A. (2012). The role of FGF signaling in guiding coordinate movement of cell groups. Guidance cue and cell adhesion regulator? *Cell Adhesion and Migration*, *6*, 397–403.

Beiman, M., Shilo, B. Z., & Volk, T. (1996). Heartless, a Drosophila FGF receptor homolog, is essential for cell migration and establishment of several mesodermal lineages. *Genes and Development*, *10*, 2993–3002.

Beira, J. V., & Paro, R. (2016). The legacy of Drosophila imaginal discs. *Chromosoma*, 125, 573-592.

Bodmer, R. (1993). The gene tinman is required for specification of the heart and visceral muscles in Drosophila. *Development*, *118*, 719–729.

517 Bour, B. A., O'Brien, M. A., Lockwood, W. L., Goldstein, E. S., Bodmer, R., Taghert, P. H.,
518 & Nguyen, H. T. (1995). Drosophila MEF2, a transcription factor that is essential for
519 myogenesis. *Genes & development*, *9*, 730-741.
520
521 Bryantsev, A. L., & Cripps, R. M. (2009). Cardiac gene regulatory networks in Drosophila.
522 *Biochimica et Biophysica Acta (BBA)-Gene Regulatory Mechanisms*, 1789, 343-353.
523
524 Campos-Ortega, J. A., & Hartenstein, V. (1985). The embryonic development of Drosophila
525 melanogaster. Berlin/Heidelberg: Springer-Verlag.
526
527 Carmena, A., Gisselbrecht, S., Harrison, J., Jiménez, F., & Michelson, A. M. (1998).
528 Combinatorial signaling codes for the progressive determination of cell fates in the Drosophila
529 embryonic mesoderm. *Genes and Development*, *12*, 3910–3922.
530
531 Ciruna, B., & Rossant, J. (2001). FGF signaling regulates mesoderm cell fate specification and
532 morphogenetic movement at the primitive streak. *Developmental cell*, 1, 37-49.
533
534 Ebisuya, M., & Briscoe, J. (2018). What does time mean in development? *Development*, 145,
535 dev164368.
536
537 Engel, F. B., Hsieh, P. C., Lee, R. T., & Keating, M. T. (2006). FGF1/p38 MAP kinase inhibitor
538 therapy induces cardiomyocyte mitosis, reduces scarring, and rescues function after myocardial
539 infarction. Proceedings of the National Academy of Sciences, 103, 15546-15551.
540
541 Fantl, W. J., Johnson, D. E., & Williams, L. T. (1993). Signaling by receptor tyrosine kinases.
542 *Annual review of biochemistry,* 62, 453-481.
543
544 Gabay, L., Seger, R., & Shilo, B. Z. (1997). MAP kinase in situ activation atlas during
545 Drosophila embryogenesis. *Development*, *124*, 3535-3541.
546
547 Gajewski, K., Kim, Y., Lee, Y. M., Olson, E. N., & Schulz, R. A. (1997). D-mef2 is a target
548 for Tinman activation during Drosophila heart development. *EMBO Journal*, *16*, 515–522.
549

550 Gisselbrecht, S., Skeath, J. B., Doe, C. Q., & Michelson, A. M. (1996). heartless encodes a
551 fibroblast growth factor receptor (DFR1/DFGF-R2) involved in the directional migration of
552 early mesodermal cells in the Drosophila embryo. *Genes and Development*, *10*, 3003–3017.
553
554 Han, Z., & Bodmer, R. (2003). Myogenic cells fates are antagonized by Notch only in
555 asymmetric lineages of the Drosophila heart, with or without cell division. *Development*, *130*,
556 3039-3051.
557
558 Ho, J., Tumkaya, T., Aryal, S., Choi, H., & Claridge-Chang, A. (2019). Moving beyond P
559 values: Everyday data analysis with estimation plots. *Nature Methods*, 16, 565-566.
560
561 House, S. L., Wang, J., Castro, A. M., Weinheimer, C., Kovacs, A., & Ornitz, D. M. (2015).
562 Fibroblast growth factor 2 is an essential cardioprotective factor in a closed-chest model of
563 cardiac ischemia-reperfusion injury. Physiological reports, 3, e12278.
564
565 Huang, A., Amourda, C., Zhang, S., Tolwinski, N. S., & Saunders, T. E. (2017). Decoding
566 temporal interpretation of the morphogen Bicoid in the early drosophila embryo. *ELife*, *6*, 1–
567 21.
568
569 Huang, A., & Saunders, T. E. (2020). A matter of time: Formation and interpretation of the
570 Bicoid morphogen gradient. *Current Topics in Developmental Biology, 137, 79-117*
571
572 Johnson, H. E., Djabrayan, N. J., Shvartsman, S. Y., & Toettcher, J. E. (2020). Optogenetic
573 rescue of a patterning mutant. *Current Biology*, 30, 3414-3424.
574
575 Johnson, H. E., Goyal, Y., Pannucci, N. L., Schüpbach, T., Shvartsman, S. Y., & Toettcher,
576 J.E. (2017). The Spatiotemporal Limits of Developmental Erk Signaling. *Developmental Cell*,
577 *40*, 185–192.
578
579 Kadam, S., McMahon, A., Tzou, P., & Stathopoulos, A. (2009). FGF ligands in Drosophila
580 have distinct activities required to support cell migration and differentiation. *Development*,
581 *136*, 739–747.
582

583 Kaur, P., Saunders, T. E., & Tolwinski, N. S. (2017). Coupling optogenetics and light-sheet
584 microscopy, a method to study Wnt signaling during embryogenesis. *Scientific Reports*, *7*, 1–
585 11.
586
587 Kim, N., Kim, J. M., Lee, M., Kim, C. Y., Chang, K. Y., & Do Heo, W. (2014). Spatiotemporal
588 control of fibroblast growth factor receptor signals by blue light. *Chemistry & biology*, 21, 903-
589 912.
590
591 Klambt, C., Glazer, L., & Shilo, B. Z. (1992). *breathless*, A Drosophila FGF receptor homolog,
592 is essential for migration of tracheal and specific midline glial cells. *Genes and Development*,
593 *6*, 1668–1678.
594
595 Korf-Klingebiel, M., Kempf, T., Schlüter, K. D., Willenbockel, C., Brod, T., Heineke, J., &
596 Drexler, H. (2011). Conditional transgenic expression of fibroblast growth factor 9 in the adult
597 mouse heart reduces heart failure mortality after myocardial infarction. Circulation, 123, 504-
598 514.
599
600 Lavoie, H., Gagnon, J., & Therrien, M. (2020). ERK signaling: a master regulator of cell
601 behaviour, life and fate. *Nature Reviews Molecular Cell Biology*, 21, 607-632.
602
603 Li, P., & Elowitz, M. B. (2019). Communication codes in developmental signaling
604 pathways. *Development*, *146*, dev170977.
605
606 Lilly, B., Zhao, B., Ranganayakulu, G., Paterson, B. M., Schulz, R. A., & Olson, E. N. (1995).
607 Requirement of MADS domain transcription factor D-MEF2 for muscle formation in
608 Drosophila. *Science*, *267*, 688-693.
609
610 Lovato, T., & Cripps, R. (2016). Regulatory Networks that Direct the Development of
611 Specialized Cell Types in the Drosophila Heart. *Journal of Cardiovascular Development and*
612 *Disease*, *3*, 18.
613

614 Mandal, L., Dumstrei, K., & Hartenstein, V. (2004). Role of FGFR signaling in the
615 morphogenesis of the Drosophila visceral musculature. *Developmental dynamics: an official*
616 *publication of the American Association of Anatomists*, 231, 342-348.
617
618 McMahon, A., Reeves, G. T., Supatto, W., & Stathopoulos, A. (2010). Mesoderm migration in
619 Drosophila is a multi-step process requiring FGF signaling and integrin activity. *Development*,
620 *137*, 2167–2175.
621
622 McMahon, A., Supatto, W., Fraser, S. E., & Stathopoulos, A. (2008). Dynamic analyses of
623 Drosophila gastrulation provide insights into collective cell migration. *Science,* 322, 1546-
624 1550.
625
626 Mele, S., & Johnson, T. K. (2020). Receptor tyrosine kinases in development: Insights from
627 drosophila. *International Journal of Molecular Sciences*, *21*, 1–21.
628
629 Michelson, A. M., Gisselbrecht, S., Buff, E., & Skeath, J. B. (1998). Heartbroken is a specific
630 downstream mediator of FGF receptor signaling in Drosophila. *Development*, *125*, 4379-4389.
631
632 Michelson, A. M., Gisselbrecht, S., Zhou, Y., Baek, K. H., & Buff, E. M. (1998). Dual
633 functions of the heartless fibroblast growth factor receptor in development of the Drosophila
634 embryonic mesoderm. *Developmental Genetics*, *22*, 212–229.
635
636 Mohammadi, M., Dikic, I., Sorokin, A., Burgess, W. H., Jaye, M., & Schlessinger, J. (1996).
637 Identification of six novel autophosphorylation sites on fibroblast growth factor receptor 1 and
638 elucidation of their importance in receptor activation and signal transduction. *Molecular and*
639 *cellular biology*, 16, 977-989.
640
641 Muha, V., & Müller, H. A. J. (2013). Functions and mechanisms of fibroblast growth factor
642 (FGF) signaling in Drosophila melanogaster. *International Journal of Molecular Sciences*, *14*,
643 5920–5937.
644
645 Ornitz, D. M., & Itoh, N. (2015). The fibroblast growth factor signaling pathway. *Wiley*
646 *Interdisciplinary Reviews: Developmental Biology,* 4, 215-266.
647

648 Perrimon, N., Pitsouli, C., & Shilo, B. Z. (2012). Signaling mechanisms controlling cell fate
649 and embryonic patterning. *Cold Spring Harbor Perspectives in Biology*, 4, a005975.
650
651 Presta, M., Chiodelli, P., Giacomini, A., Rusnati, M., & Ronca, R. (2017). Fibroblast growth
652 factors (FGFs) in cancer: FGF traps as a new therapeutic approach. *Pharmacology &*
653 *therapeutics*, *179*, 171-187.
654
655 Reichman-Fried, M., & Shilo, B. Z. (1995). Breathless, a Drosophila FGF receptor homolog,
656 is required for the onset of tracheal cell migration and tracheole formation. *Mechanisms of*
657 *Development*, *52*, 265–273.
658
659 Reim, I., & Frasch, M. (2010). Genetic and genomic dissection of cardiogenesis in the
660 *Drosophila* model. *Pediatric Cardiology*, *31*, 325–334.
661
662 Roskoski Jr, R. (2019). Targeting ERK1/2 protein-serine/threonine kinases in human cancers.
663 *Pharmacological research,* 142, 151-168.
664
665 Sagner, A., & Briscoe, J. (2017). Morphogen interpretation: concentration, time, competence,
666 and signaling dynamics. *Wiley Interdisciplinary Reviews: Developmental Biology*, *6*, e271.
667
668 Schwarz, B., Hollfelder, D., Scharf, K., Hartmann, L., & Reim, I. (2018). Diversification of
669 heart progenitor cells by EGF signaling and differential modulation of ETS protein activity.
670 *ELife*, *7*, 1–36.
671
672 Shishido, E., Ono, N., Kojima, T., & Saigo, K. (1997). Requirements of DFR1/Heartless, a
673 mesoderm-specific Drosophila FGF-receptor, for the formation of heart, visceral and somatic
674 muscles, and ensheathing of longitudinal axon tracts in CNS. *Development*, *124*, 2119–2128.
675
676 Sopko, R., & Perrimon, N. (2013). Receptor tyrosine kinases in Drosophila development. *Cold*
677 *Spring Harbor Perspectives in Biology*, *5*, 1–32.
678
679 Spivak-Kroizman, T., Lemmon, M. A., Dikic, I., Ladbury, J. E., Pinchasi, D., Huang, J., ... &
680 Lax, I. (1994). Heparin-induced oligomerization of FGF molecules is responsible for FGF
681 receptor dimerization, activation, and cell proliferation. *Cell,* 79, 1015-1024.

682

683 Stathopoulos, A., Tam, B., Ronshaugen, M., Frasch, M., & Levine, M. (2004). Pyramus and
684 thisbe: FGF genes that pattern the mesoderm of Drosophila embryos. *Genes and Development*,
685 *18*, 687–699.
686

687 Teven, C. M., Farina, E. M., Rivas, J., & Reid, R. R. (2014). Fibroblast growth factor (FGF)
688 signaling in development and skeletal diseases. *Genes and Diseases*, *1*, 199–213.
689

690 Thisse, B., & Thisse, C. (2005). Functions and regulations of fibroblast growth factor signaling
691 during embryonic development. *Developmental Biology*, *287*, 390–402.
692

693 Turner, N., & Grose, R. (2010). Fibroblast growth factor signaling: from development to
694 cancer. *Nature Reviews Cancer*, *10*, 116-129.
695

696 Vincent, S., Wilson, R., Coelho, C., Affolter, M., & Leptin, M. (1998). The Drosophila protein
697 Dof is specifically required for FGF signaling. *Molecular Cell*, *2*, 515–525.
698

699 Viswanathan, R., Necakov, A., Trylinski, M., Harish, R. K., Krueger, D., Esposito, E., … De
700 Renzis, S. (2019). Optogenetic inhibition of Delta reveals digital Notch signaling output during
701 tissue differentiation. *EMBO Reports*, *20*, e47999.
702

703 Vogler, G., & Bodmer, R. (2015). Cellular Mechanisms of Drosophila Heart Morphogenesis.
704 *Journal of Cardiovascular Development and Disease*, *2*, 2–16.
705

706 Wangler, M. F., Yamamoto, S., & Bellen, H. J. (2015). Fruit flies in biomedical research.
707 *Genetics,* 199, 639-653.
708

709 Wartlick, O., Mumcu, P., Jülicher, F., & Gonzalez-Gaitan, M. (2011). Understanding
710 morphogenetic growth control—lessons from flies. *Nature Reviews Molecular Cell Biology*,
711 12, 594-604.
712

713 Wesche, J., Haglund, K., & Haugsten, E. M. (2011). Fibroblast growth factors and their
714 receptors in cancer. *Biochemical Journal*, *437*, 199-213.
715

Wilson, R., & Leptin, M. (2000). Fibroblast growth factor receptor-dependent morphogenesis of the Drosophila mesoderm. *Philosophical Transactions of the Royal Society B: Biological Sciences*, *355*, 891–895.

Wilson, R., Vogelsang, E., & Leptin, M. (2005). FGF signaling and the mechanism of mesoderm spreading in Drosophila embryos. *Development*, *132*, 491–501.

Xie, Y., Su, N., Yang, J., Tan, Q., Huang, S., Jin, M., ... & Chen, H. (2020). FGF/FGFR signaling in health and disease. Signal Transduction and Targeted Therapy, 5, 1-38.

Yin, J., Lee, R., Ono, Y., Ingham, P. W., & Saunders, T. E. (2018). Spatiotemporal coordination of FGF and Shh signaling underlies the specification of myoblasts in the zebrafish embryo. *Developmental cell*, 46, 735-750.

Yu, X., Sayegh, R., Maymon, M., Warpeha, K., Klejnot, J., Yang, H., ... & Lin, C. (2009). Formation of nuclear bodies of Arabidopsis CRY2 in response to blue light is associated with its blue light–dependent degradation. *The Plant Cell*, 21, 118-130.

Zhang, S., Amourda, C., Garfield, D., & Saunders, T. E. (2018). Selective filopodia adhesion ensures robust cell matching in the Drosophila heart. *Developmental Cell*, *46*, 189-203.

Zhang, S., Teng, X., Toyama, Y., & Saunders, T. E. (2020). Periodic Oscillations of Myosin-II Mechanically Proofread Cell-Cell Connections to Ensure Robust Formation of the Cardiac Vessel. *Current Biology, 70, 3364.*

Zhou, Y., Popadowski, S. E., Deutschman, E., & Halfon, M. S. (2019). Distinct roles and requirements for Ras pathway signaling in visceral versus somatic muscle founder specification. *Development*, *146*, dev169003.

Zinner, M., Lukonin, I., & Liberali, P. (2020). Design principles of tissue organisation: How single cells coordinate across scales. *Current Opinion in Cell Biology*, *67*, 37-45.

749 **Figures:**

750

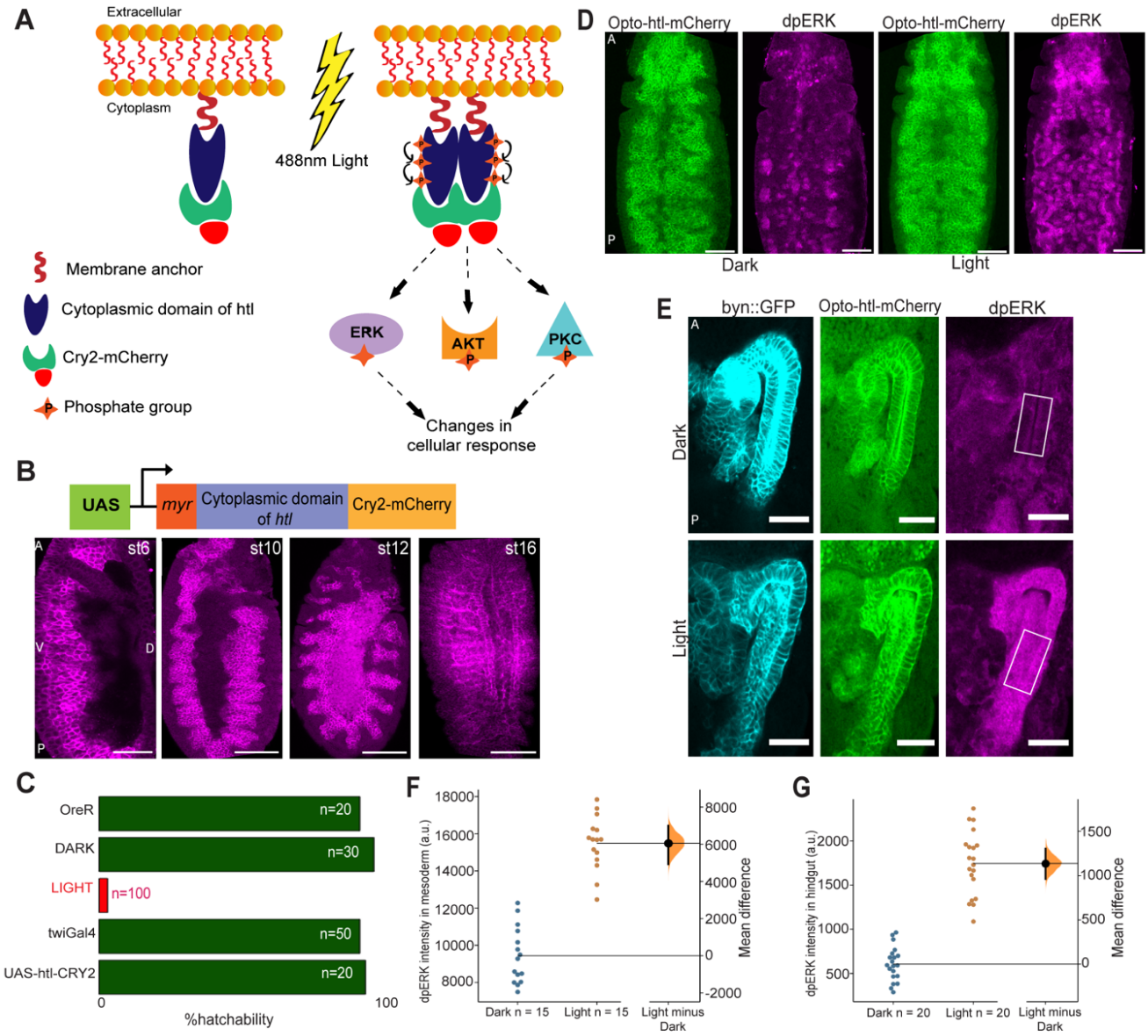

751

752 **Fig. 1 Opto-htl expression and activation in different tissues**

753 A) Schematic showing design and activation of Opto-htl. Exposure to 488nm light induces
754 CRY2 clustering leading to activation of the (intracellular) membrane-bound receptor and
755 eventually generating a cellular response via phosphorylation of various downstream target
756 molecules. B) Twi-Gal4>Opto-htl embryos stained with anti-mCherry antibody showing the
757 expression of the construct at various stages. C) Hatchability assay for different genetic
758 conditions. OreR = OregonR, DARK = Twi-Gal4>Opto-htl embryos kept under illumination
759 with amber paper to block 488nm wavelengths throughout development, LIGHT = Twi-
760 Gal4>Opto-htl embryos kept under illumination throughout development. Twi-Gal4 embryos

represent the Gal4 driver alone. UAS-htl-Cry2-mCherry represents Opto-htl embryos with no Gal4 driver. D) Twi-Gal4>Opto-htl embryos fixed and stained at late stage 10/early stage 11 for pErk under dark and light conditions. E) Byn-GAL4>Opto-htl embryos fixed and stained at stage 16 for pErk under dark and light conditions (scale bar 25μm). F) pErk intensity differences in the mesoderm at late stage 10 between Twi-Gal4>Opto-htl embryos kept under dark versus light. G) pErk intensity differences in the hindgut between Byn-GAL4>Opto-htl embryos under dark and light conditions in stage 16 measured in the region shown in (E). Scale bar = 50μm unless stated otherwise. A = Anterior, P = Posterior, D = Dorsal, V = Ventral view. In (F,G), the black bar represents the 95% confidence interval with the Bootstrap distribution shown in orange (see Ho *et al.,* 2019 for details).

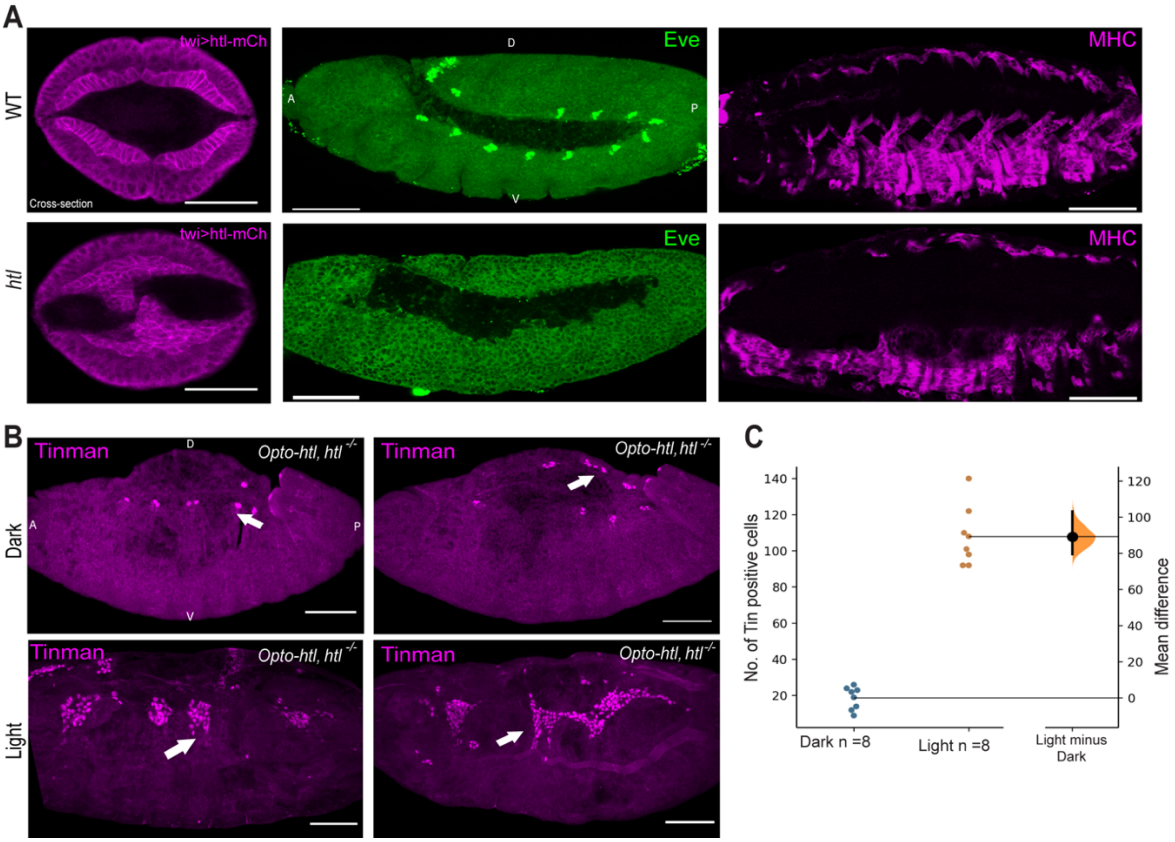

Fig. 2 Rescue of *htl* mutant using Opto-htl

A) Comparison between wild-type and *htl* homozygous mutant embryos at different stages: Mesoderm spreading (stage 10), Eve-positive pericardial precursor cells (stage 11) and muscles marked by Myosin staining (stage 15). B) Twi-Gal4>Opto-htl is expressed against *htl* null background and embryos illuminated and stained with Tin antibody. Two homozygous mutants are compared under dark and light conditions for Tin-positive cells. C) Quantification of the number of Tin-positive cells in dark and light conditions for embryos as described in (B). Scale bar = 50µm. A = Anterior, P = Posterior, D = Dorsal, V = Ventral view. In (C), the black bar represents the 95% confidence interval with the Bootstrap distribution shown in orange (see Ho *et al*., 2019 for details).

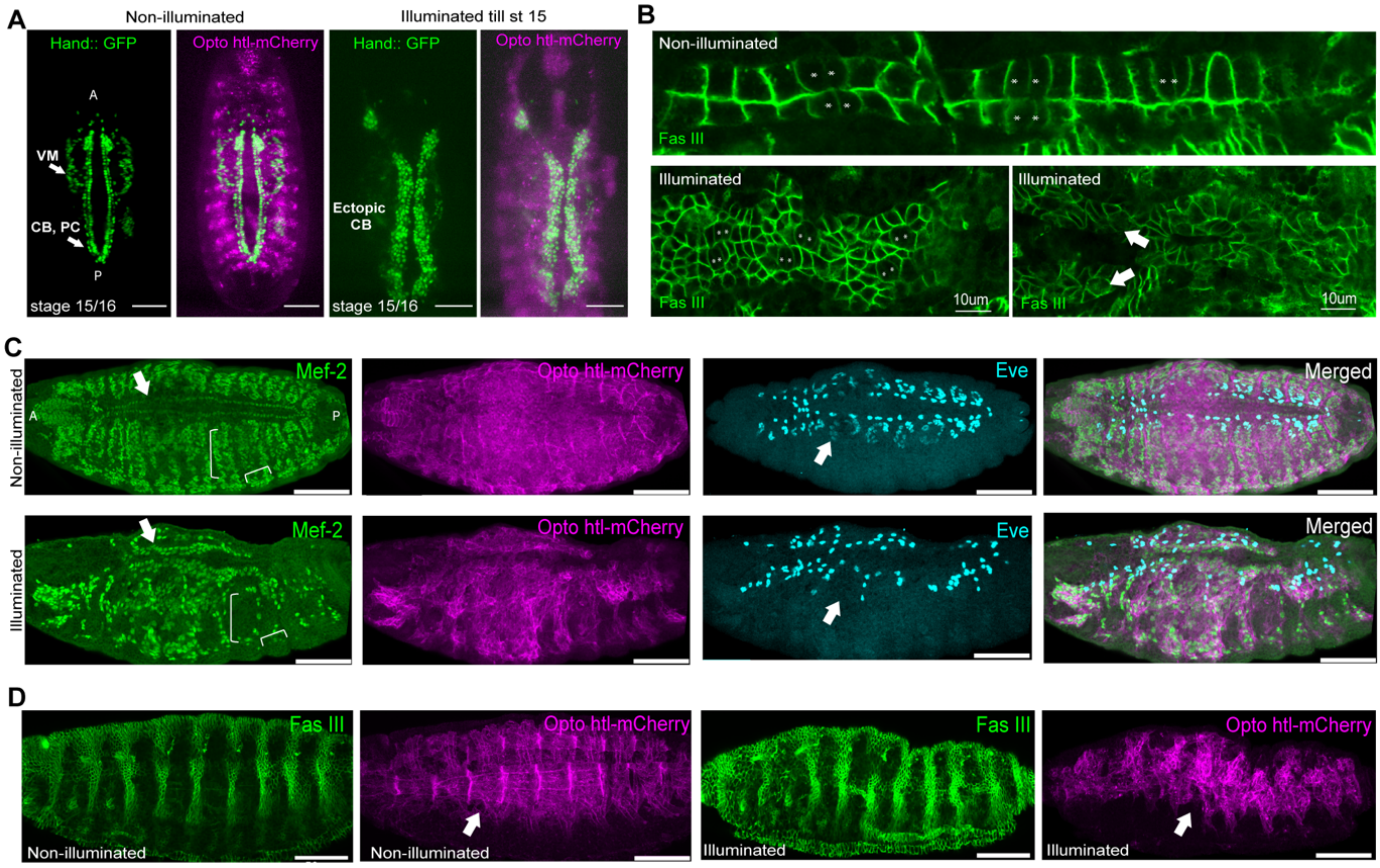

Fig. 3 Mesoderm specific defects in Twi-GAL4> UAS - htl-CRY2-mCherry embryos kept under constant light

(A) Twi-GAL4>Hand::GFP;Opto-htl embryos kept under dark and illuminated conditions, imaged using a light-sheet at stage 15 (Opto-htl signal in magenta). (B) Twi-GAL4>Opto-htl embryos stained with Fas3 and imaged at stage 16 under dark conditions (top) and when illuminated by constant 488nm light (bottom). Svp-positive cells, marked with an asterisk, are identified by lower Fas3 expression. Arrows denote branching of the heart structure. (C) Twi-GAL4>Opto-htl embryos stained with Mef-2 and Eve antibodies at stage 16 under dark and illumination conditions. Arrows correspond to phenotypes described in the text. (D) Muscle structure in Twi-GAL4>Opto-htl embryos kept under dark and light conditions visualised using Opto-htl-mCherry. Scale bar = 50µm unless stated otherwise.

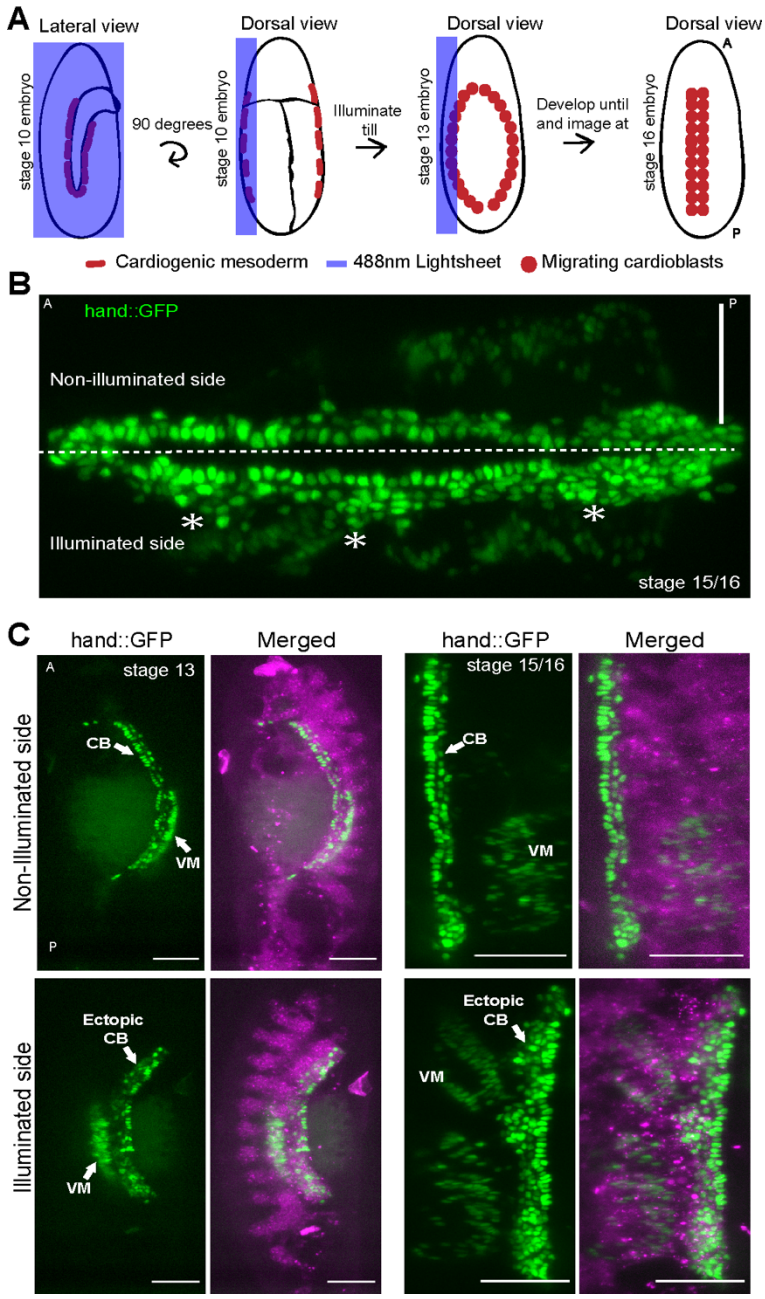

Fig. 4 Spatial control of Opto-htl activation

A) Schematic of the imaging protocol for half-illumination of embryos on a light-sheet microscope. B) Dorsal view of a Twi-Gal4>hand::GFP;Opto-htl embryo illuminated as described in (A) and imaged at stage 16. C) Non-illuminated (top row) and illuminated (bottom row) sides of a Twi-Gal4>hand::GFP;Opto-htl embryo. Left panels, stage 13. Right panels, stage 15/16. VM= Visceral mesoderm, CB= Cardioblasts, PC= Pericardial cells. Scale bar = 50µm.

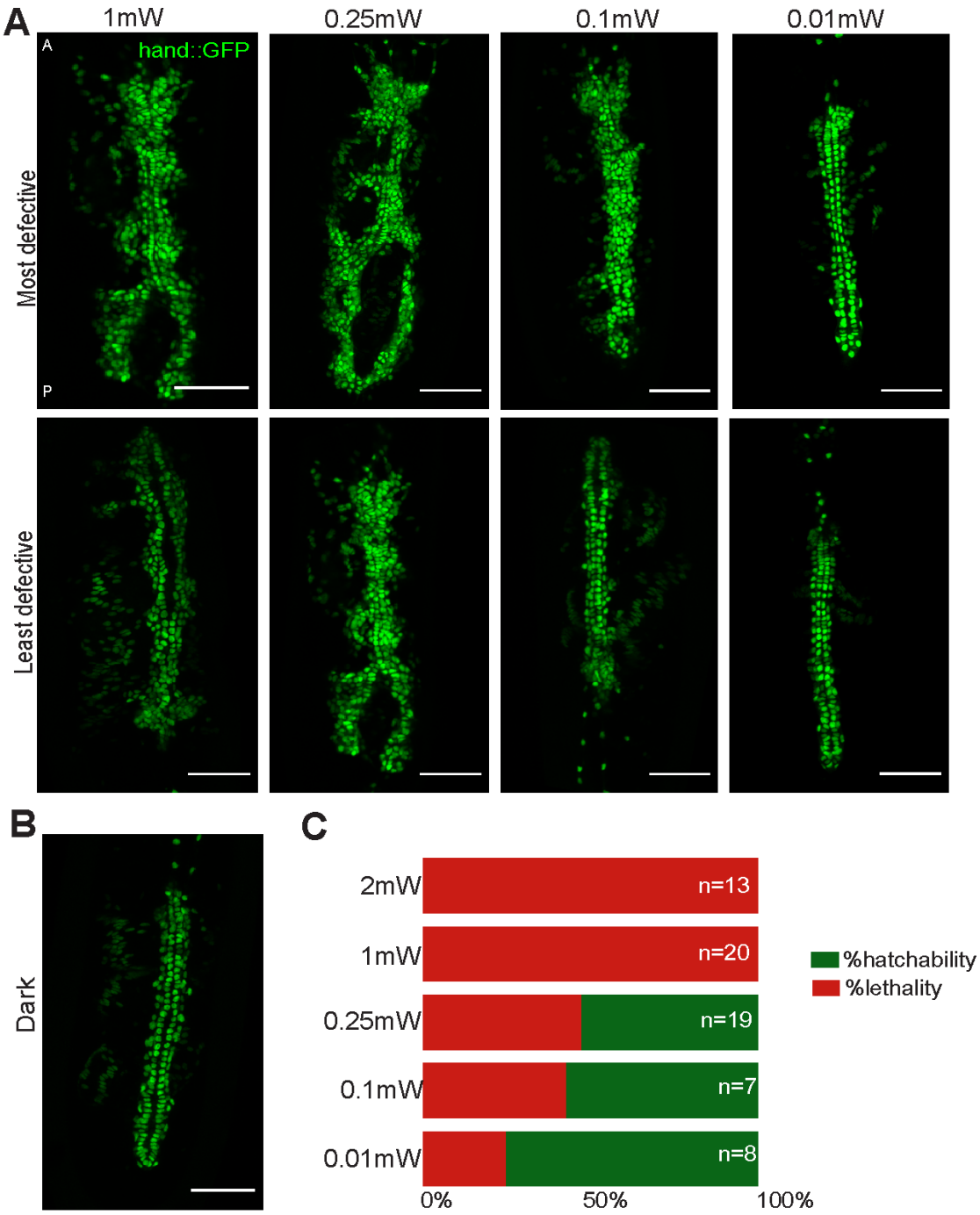

Fig. 5 Opto-htl induced phenotype depends on light intensity

A) Representative images of the heart at stage 16 in Twi-Gal4>hand::GFP;Opto-htl embryos illuminated from stage 5 till stage 16, at different light intensities. B) Heart at stage 16 in a Twi-Gal4>hand::GFP;Opto-htl embryo kept in the dark through development. C) Survival rate of Twi-Gal4>Opto-htl embryos when illuminated at different intensities throughout development. Scale bar = 50µm.

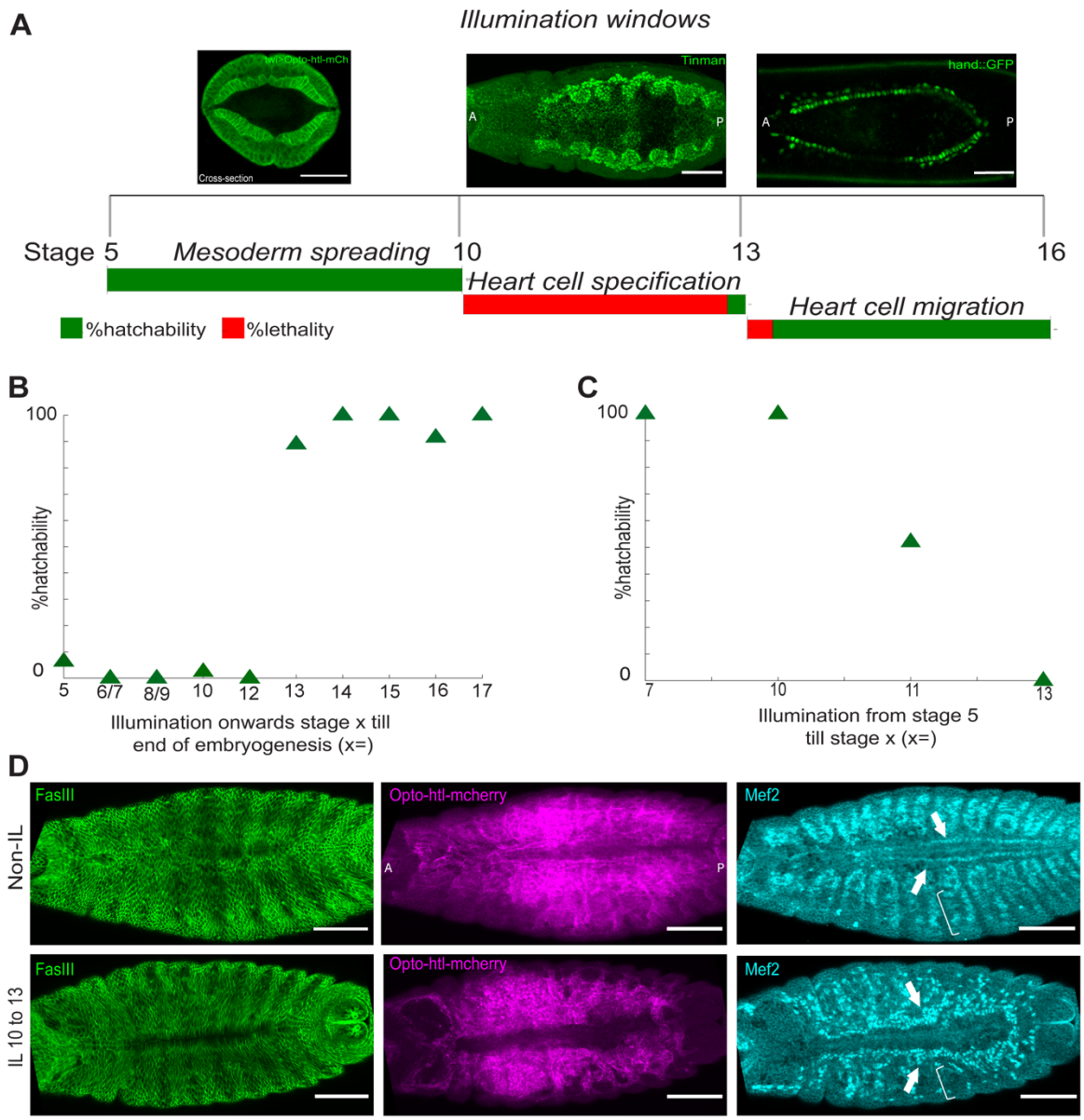

853

854 **Fig. 6 Temporal control of Opto-htl activation during development**

855 A) Hatchability assay for Twi-GAL4>Opto-htl embryos illuminated during different time
856 windows during development. (Top) Representative images of the embryo stage being
857 illuminated. (Bottom) Hatching percentage, with the length of each bar representing 100%. B)
858 Hatchability of Twi-GAL4>Opto-htl embryos when illuminated from the specified stage on
859 the x-axis to the end of embryogenesis C) Hatchability of Twi-GAL4>Opto-htl embryos when
860 illuminated from stage 5 until the specified stage on the x-axis (see Table 2A-B for embryo
861 count) D) Twi-GAL4>Opto-htl embryos stained with Fas3, Mef2 and mCherry antibodies
862 under different illumination conditions. Arrowheads point towards Mef-2 marked cardioblasts.
863 Scale bars = 50μm.

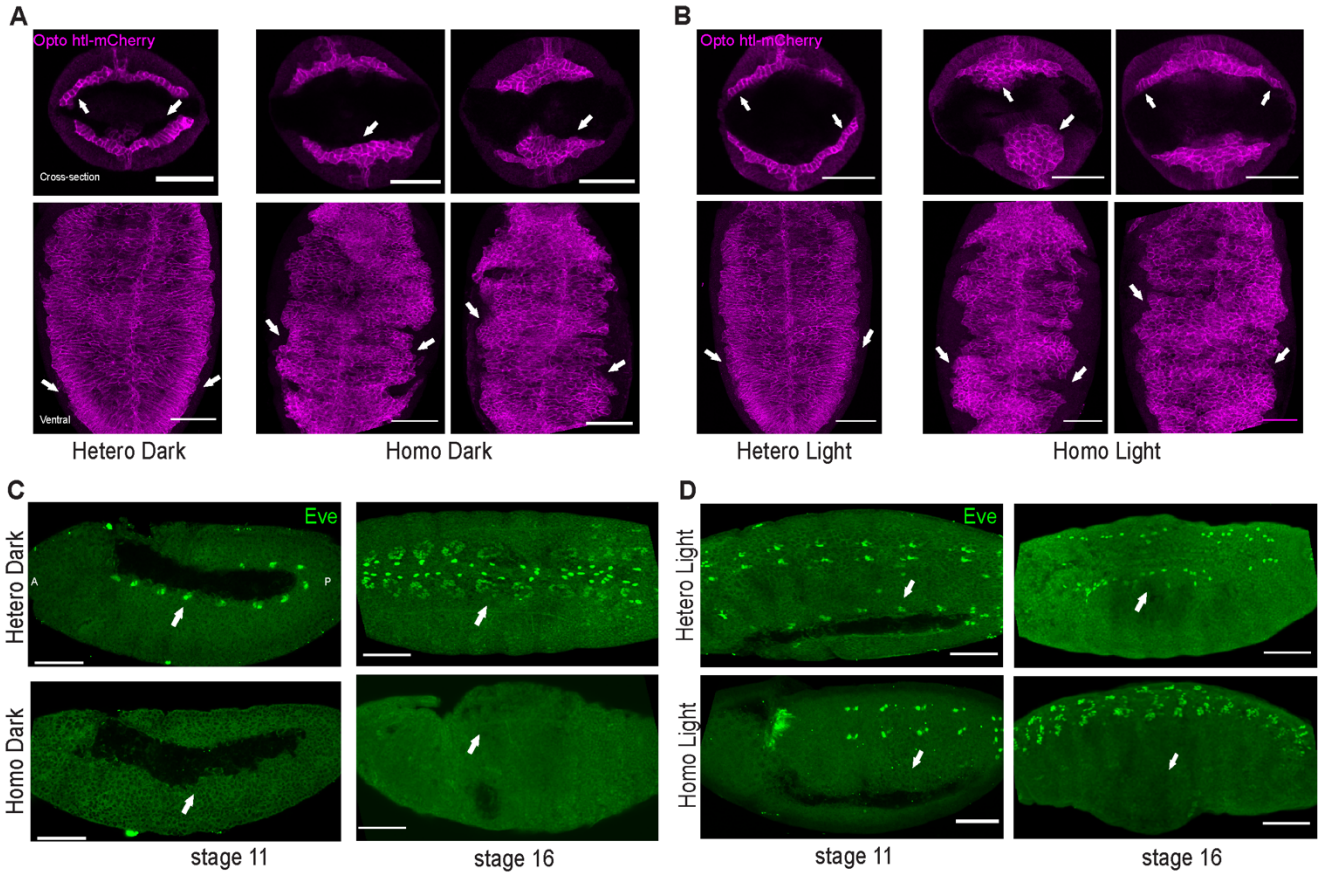

Supplementary Fig. 1 Rescue phenotypes using UAS-Opto-htl

A) Mesoderm spreading in heterozygous and homozygous *htl* mutant embryos kept under dark conditions, imaged at the cross-section (top row) and from the ventral side (bottom row). B) Mesoderm spreading in heterozygous and homozygous *htl* mutant embryos illuminated from stage 5 till stage 10. Upon illumination, homozygous mutants expressing Opto-htl exhibit clustering of mesoderm cells and non-uniform spreading with flattening observed occasionally in some regions. No rescue of Eve-positive cells is observed in the homozygous mutants under light either at stage 11 (C) or stage 16 (D). Scale bar = 50μm.

875

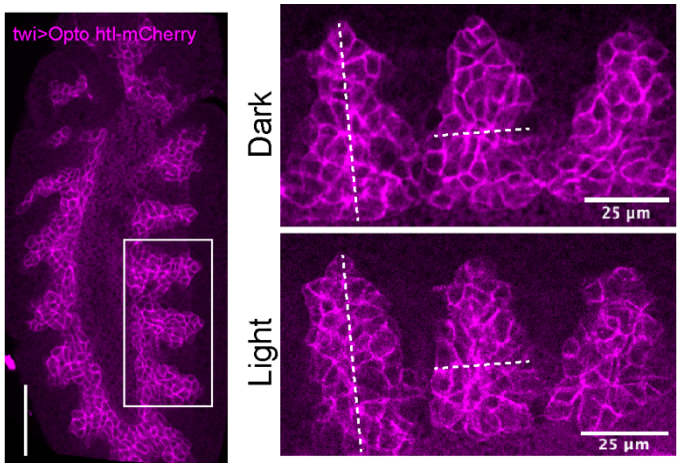

876 **Supplementary Fig. 2 Mesodermal cells in Opto-htl embryos**

877 Twi-Gal4>Opto-htl-mCherry embryos fixed and stained at stage 11 with anti-mCherry
878 antibody under dark and light conditions. No expansion of mesodermal cells is observed upon
879 light activation. Scale bar = 50µm unless stated otherwise.

880

881

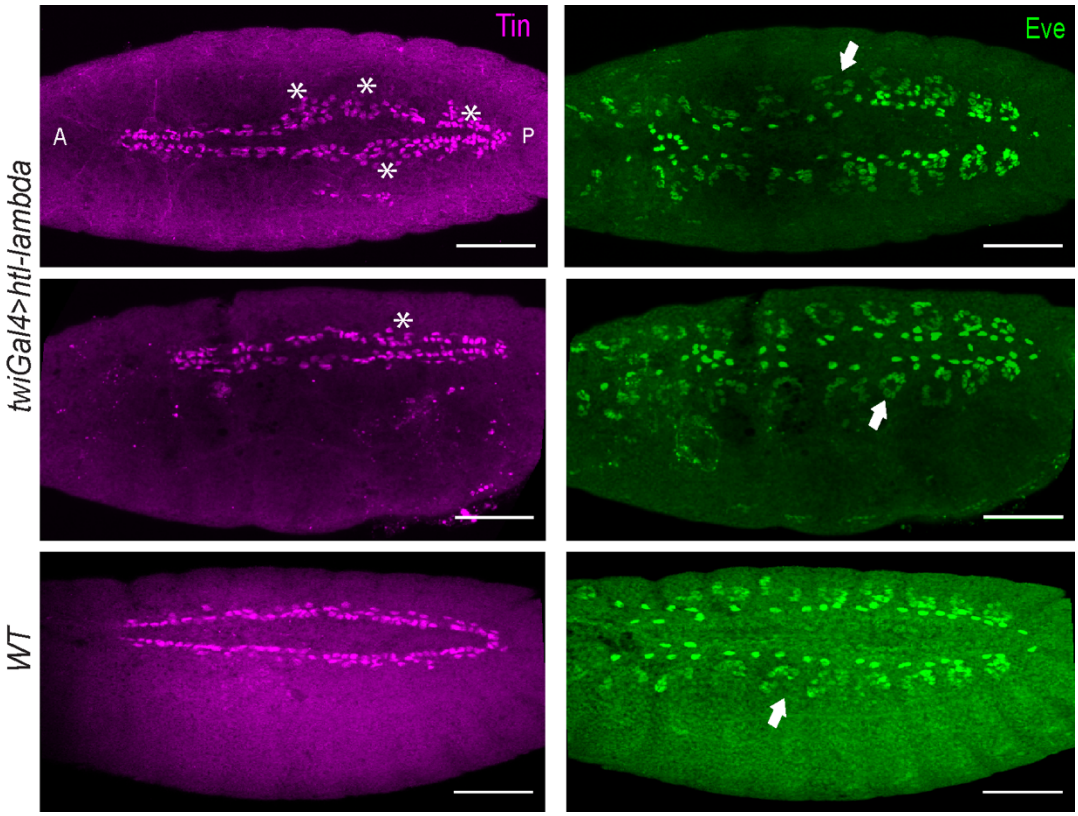

882 **Supplementary Fig. 3 htl-λ activation in the mesoderm**

883 Dorsal view of Twi-Gal4>UAS-htl-λ embryos fixed and stained at stage 15 with Tin and Eve
884 antibody, compared with WT embryos at the same stage. Asterisks represent ectopic tin cells.
885 Arrowhead point towards eve-positive DA1 muscles and pericardial cells in a given hemi
886 segment. Scale bar = 50µm.

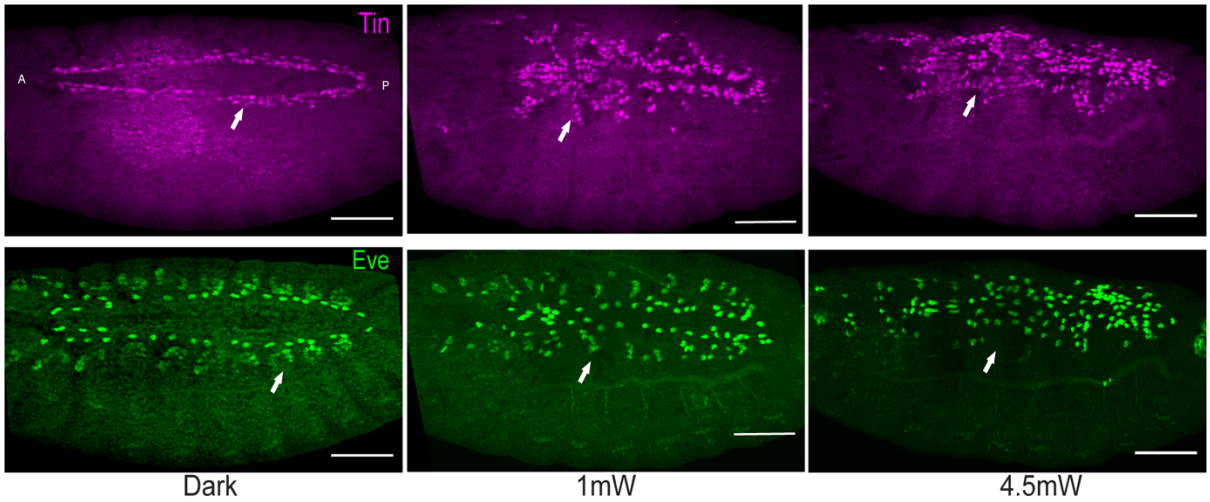

887

888 **Supplementary Fig. 4 Opto-SOS activation in the mesoderm**

889 Dorsal view of Twi-Gal4>UAS-Opto-SOS embryos fixed and stained at stage 16 with Tin and
890 Eve antibody. Embryos kept under dark show normal heart development with Tin and Eve
891 patterns similar to wild-type. Embryos illuminated at 1mW and 4.5mW light intensity from
892 stage 5 till stage 16 show a progressive increase in both Tin and Eve positive cells with a
893 complete loss of the DA1 muscle group (arrowheads) at 4.5mW intensity. Scale bar = 50µm.

894

Condition/Genotype	Mef2-CB	Eve-PC	DA1
OreR (n=12)	12	4	2
DARK-twi>Opto-htl (n=10)	12	4	2
Light-twi>Opto-htl (n=10)	29	6	0
	32	7	0
	41	9	0
	26	3	0
	20	6	0
	31	7	0
	30	6	0
	27	7	0
	21	3	0
	23	4	0

895

896 **Table 1:** Number of Mef2-positive cardioblasts, Eve-positive pericardial cells and DA1
897 muscles in OreR, Twi-Gal4>Opto-htl (dark) and Twi-Gal4>Opto-htl (illuminated) embryos.
898 Cells were counted at stage 15/16 from hemisegments A3-A4.

899

Illumination onwards stage x till hatching (stage x =)	Illumination time from cellularization stage	Stage Hallmark	No. of embryos screened	No. of embryos hatched	% hatchability
5	0 mins	Cellularisation	31	2	6.4
6/7	40 mins	Gastrulation	7	0	0
8/9	1-2:10 h	Germ band Elongation starts	5	0	0
10	2:10 h	Germ band Elongation finishes	40	1	2.5
12	5:10 h	Germ Band retraction starts	34	0	0
13	7:10 h	Midgut primordium forms a sack	19	17	89
14	8:10 h	Head Involution and DC starts	11	11	100
15	9:10 h	Dorsal Closure	18	18	100
16	11 h	Gut constrictions appear	12	11	91.6
17	14 h	First movements start; Trachea filling	16	16	100

900

901 **Table 2A:** Hatchability of Twi-GAL4>Opto-htl embryos illuminated from specified stages
902 until end of embryogenesis.

Illumination During stage	Illumination time	No. of embryos screened	No. of embryos hatched	% hatchability
5 till end of stage 7	40 min	7	7	100
5 till end of stg 10	2.5h	7	7	100
5 till end of stg 11	5 h	17	9	52
5 till end of stage 13	8 h	24	0	0

903

904 **Table 2B:** Hatchability of Twi-GAL4>Opto-htl embryos illuminated during different time
905 windows.

906 **Movie Legends:**

907

908 **Supplementary Movie 1: Opto-htl expression in the mesoderm during embryogenesis**

909 Twi-Gal4>Opto-htl embryo scanned with 561nm laser at 3 min intervals from stage 5 until end
910 of embryogenesis to visualise expression of Opto-htl.

911

912 **Supplementary Movie 2: Hatchability score for Opto-htl embryos under dark conditions**

913 Twi-Gal4>Opto-htl embryos imaged on a stereoscope covered with amber paper (to block
914 488nm light) from stage 5 until hatching. (Dark condition).

915

916 **Supplementary Movie 3: Hatchability score for Opto-htl embryos under constant**
917 **illumination**

918 Twi-Gal4>Opto-htl embryos imaged on a stereoscope from stage 5 until end of embryogenesis
919 using a 488nm light intensity of 1mW measured at the sample plane. (Light condition).

920

921 **Supplementary Movie 4: Cardioblast migration and matching in Opto-htl embryo kept**
922 **under dark conditions**

923 Twi-Gal4>hand::GFP; Opto-htl embryo kept under dark condition until stage 13 and then
924 imaged to visualise the migration of the GFP positive heart cells until matching at stage 16.

925

926 **Supplementary Movie 5: Cardioblast migration and matching in Opto-htl embryo**
927 **illuminated with 488nm laser**

928 Twi-Gal4>hand::GFP;Opto-htl embryos illuminated with 488nm laser from late stage 10 until
929 early stage 13 and then imaged using a light-sheet microscope to visualise the migration of the
930 GFP positive heart cells until matching at stage 16. (a) represents dorsal view; (b) and (c)
931 represent lateral views of the same embryo.

932

933 **Sequences and Primers:**

934

935 **Myr signal sequence (src42A)**

936

937 ATGGGTAACTGCCTCACCACACAGAAGGGCGAACCCGACAAGCCCGCA

938

939

940 **Htl FGF cytoplasmic region (Amino acid position 331-729)**

941 (Ref. http://www.uniprot.org/uniprot/Q07407)

942

943 TATGCCATCCGAAAGATGAAACATGAAAAGGTGTTGAAACAACGCATCGAAACCGTTCACCAGTGGACCAAGAAAGTGAT
944 CATCTTCAAGCCCGAAGGTGGCGGAGACTCCAGTGGTTCCATGGACACCATGATTATGCCGGTGGTTAGGATACAGAAAC
945 AGCGCACCACTGTTCTTCAGAATGGCAACGAGCCGGCTCCATTCAATGAATATGAATTTCCACTGGACTCGAACTGGGAA
946 CTGCCCAGAAGTCATTTGGTACTGGGTGCCACTTTGGGAGAAGGTGCTTTCGGACGAGTGGTCATGGCGGAGGTCAATAA
947 TGCCATTGTCGCCGTGAAAATGGTGAAGGAAGGACACACGGATGATGACATTGCCAGCTTGGTGCGGGAAATGGAAGTGA
948 TGAAGATCATTGGGCGACATATCAATATTATTAACTTACTTGGTTGCTGCAGTCAAAATGGTCCGCTCTATGTGATTGTC
949 GAGTATGCGCCACACGGAAATCTCAAGGACTTCCTCTATAAAAATCGACCCTTCGGAAGGGATCAGGATAGGGACAGCTC
950 GCAACCGCCGCCATCGCCACCAGCTCATGTGATAACCGAAAAGGATCTGATCAAATTTGCCCACCAAATTGCCAGAGGAA
951 TGGACTATTTGGCCTCGCGGCGATGCATCCATCGAGATTTGGCAGCCAGGAATGTGCTCGTCAGCGATGATTATGTGCTG
952 AAGATTGCTGATTTTGGACTGGCGAGGGACATTCAAAGCACGGATTACTATCGGAAGAACACAAATGGCAGGCTACCCAT
953 CAAATGGATGGCACCGGAGTCGCTGCAGGAGAAATTCTATGATTCCAAGAGCGATGTCTGGTCATATGGCATCCTGCTGT
954 GGGAGATCATGACCTATGGGCAGCAACCATATCCAACTATCATGTCCGCTGAGGAGCTGTACACCTATCTCATGTCCGGT
955 CAGCGGATGGAGAAACCAGCGAAATGCTCCATGAACATCTACATTCTGATGCGACAATGTTGGCATTTCAACGCCGACGA
956 TCGGCCACCTTTTACGGAAATTGTTGAGTATATGGACAAGCTGCTCCAGACGAAGGAGGACTACCTCGATGTGGATATCG
957 CCAATCTGGATACACCGCCCTCGACTAGCGACGAGGAGGAAGATGAAACGGACAACCTGCAGAAGTGGTGTAATTAT

958

959

960 **CRY2mcherry (Ref. Addgene26866)**

961

962 atgaagatggacaaaaagactatagtttggtttagaagagacctaaggattgaggataatcctgcattagcagcagctgc
963 tcacgaaggatctgtttttcctgtcttcatttggtgtcctgaagaagaaggacagttttatcctggaagagcttcaagat
964 ggtggatgaaacaatcacttgctcacttatctcaatccttgaaggctcttggatctgacctcactttaatcaaaacccac
965 aacacgatttcagcgatcttggattgtatccgcgttaccggtgctacaaaagtcgtctttaaccacctctatgatcctgt
966 ttcgttagttcgggaccataccgtaaaggagaagctggtggaacgtgggatctctgtgcaaagctacaatggagatctat
967 tgtatgaaccgtgggagatatactgcgaaaagggcaaacctttacgagtttcaattcttactggaagaaatgcttagat
968 atgtcgattgaatccgttatgcttcctcctccttggcggttgatgccaataactgcagcggctgaagcgatttgggcgtg
969 ttcgattgaagaactagggctggagaatgaggccgagaaaccgagcaatgcgttgttaactagagcttggtctccaggat
970 ggagcaatgctgataagttactaaatgagttcatcgagaagcagttgatagattatgcaaagaacagcaagaaagttgtt
971 gggaattctacttcactactttctccgtatctccatttcggggaaataagcgtcagacacgttttccagtgtgcccggat
972 gaaacaaattatatgggcaagagataagaacagtgaaggagaagaaagtgcagatctttttcttaggggaatcggtttaa
973 gagagtattctcggtatatatgtttcaacttcccgtttactcacgagcaatcgttgttgagtcatcttcggtttttccct
974 tgggatgctgatgttgataagttcaaggcctggagacaaggcaggaccggttatccgttggtggatgccggaatgagaga
975 gctttgggctaccggatggatgcataacagaataagagtgattgtttcaagctttgctgtgaagtttcttctccttccat
976 ggaaatggggaatgaagtatttctgggatacacttttggatgctgatttggaatgtgacatccttggctggcagtatatc
977 tctgggagtatccccgatggccacgagcttgatcgcttggacaatcccgcgttacaaggcgccaaatatgacccagaagg
978 tgagtacataaggcaatggcttcccgagcttgcgagattgccaactgaatggatccatcatccatgggacgctcctttaa
979 ccgtactcaaagcttctggtgtggaactcggaacaaactatgcgaaacccattgtagacatcgacacagctcgtgagcta
980 ctagctaaagctatttcaagaacccgtgaagcacagatcatgatcggagcagcaGCCCGGGATCCACCGGTCGCCACCAT
981 GGTGAGCAAGGGCGAGGAGGATAACATGGCCATCATCAAGGAGTTCATGCGCTTCAAGGTGCACATGGAGGGCTCCGTGA
982 ACGGCCACGAGTTCGAGATCGAGGGCGAGGGCGAGGGCCGCCCCTACGAGGGCACCCAGACCGCCAAGCTGAAGGTGACC
983 AAGGGTGGCCCCCTGCCCTTCGCCTGGGACATCCTGTCCCCTCAGTTCATGTACGGCTCCAAGGCCTACGTGAAGCACCC
984 CGCCGACATCCCCGACTACTTGAAGCTGTCCTTCCCCGAGGGCTTCAAGTGGGAGCGCGTGATGAACTTCGAGGACGGCG
985 GCGTGGTGACCGTGACCCAGGACTCCTCCCTGCAGGACGGCGAGTTCATCTACAAGGTGAAGCTGCGCGGCACCAACTTC
986 CCCTCCGACGGCCCCGTAATGCAGAAGAAGACCATGGGCTGGGAGGCCTCCTCCGAGCGGATGTACCCCGAGGACGGCGC
987 CCTGAAGGGCGAGATCAAGCAGAGGCTGAAGCTGAAGGACGGCGGCCACTACGACGCTGAGGTCAAGACCACCTACAAGG
988 CCAAGAAGCCCGTGCAGCTGCCCGGCGCCTACAACGTCAACATCAAGTTGGACATCACCTCCCACAACGAGGACTACACC
989 ATCGTGGAACAGTACGAACGCGCCGAGGGCCGCCACTCCACCGGCGGCATGGACGAGCTGTACAAGTAA

990

991

992 **Primers for amplifying FGF cytoplasmic region**

993

994 FP 5'- GAACCCGACAAGCCCGCATATGCCATCCGAAAGATGAAAC -3'

995

996 RP 5'-ctttttgtccatcttcatATAATTACACCACTTCTGCAGGTTGTC-3'

997 **Primers for amplifying CRY2-mcherry**
998
999 FP- 5'-CAGAAGTGGTGTAATTATatgaagatggacaaaaagactatagtttgg-3'
1000
1001 RP 5'- GGGGTGCCTAATGCGGCCGCTTACTTGTACAGCTCGTCCATGC -3'
1002
1003
1004 **Myr sequence synthesized**
1005
1006 5'-GGTATACACCTAGGCGGTACCATGGGTAACTGCCTCACCACACAGAAGGGCGAACCCGACAAGCCCGCATATGCCATCCG
1007 AAAGATG-3'
1008
1009 3'-CCATATGTGGATCCGCCATGGTACCCATTGACGGAGTGGTGTGTCTTCCCGCTTGGGCTGTTCGGGCGTATACGGTAGGC
1010 TTTCTAC-5'